HAINING ZHANG[1], SEUNG KI MOON[2], MIN-KYO JUNG[3], PIL-HO LEE[3],
TAEHO HA[3], JOON PHIL CHOI[3*]

CONDUCTIVITY AND FLEXIBILITY ENHANCEMENT OF AEROSOL-JET-PRINTED SENSORS USING A SILVER NANOPARTICLE INK WITH CARBON NANOTUBES

Efforts to miniaturize and customize electronic devices have attracted considerable amounts of attention in many industrial fields. Recently, due to its innovative printing technology with the capability of printing fine features onto non-planar substrates without masks, aerosol jet printing (AJP) is emerging as a promising printed-electronics technology capable of meeting the requirements of various advanced electronic applications. In this research, a novel manufacturing process based on AJP is proposed in order to fabricate highly flexible and conductive customized temperature sensors. To improve the flexibility and conductivity of the printed tracks, a silver nanoparticle/carbon nanotubes composite ink is developed. Customized temperature sensors are then designed and fabricated based on the optimized process parameters of AJP. It was found that the CNTs served as bridges to connect silver nanoparticles and defects, which could be expected to reduce the contact resistivity and enhance the flexibility of the printed sensor.

Keywords: Aerosol jet printing; Direct writing; Printed sensors; Carbon nanotubes

1. Introduction

As noncontact ink writing technologies have demonstrated remarkable progress in the fine-line patterning and multilayering of microelectronics, they have been extensively adopted to fabricate various electronic devices and sensors, including transistors for driving functionalized circuits [1,2], solar cells for energy harvesting [3,4], and resistive sensors [5,6]. Aerosol jet printing (AJP) technology has been developed for producing customized and conformal microelectronic components on various flexible substrates [7,8]. As the AJP technology can be used without masks to print fine features (below 10 µm) onto non-planar substrates, it is promising in that it can meet the requirements of a range of advanced electronic applications [9,10]. Accordingly, AJP technology has been adopted as a potential solution for the miniaturization and customization of electronic devices.

Despite the fact that AJP technology is capable of the direct writing of customized and conformal microelectronic components on various flexible substrates, the performance of the fabricated electronic components is still associated with several drawbacks. Compared to the electrical resistivity of bulk metal materials, the printed nanoparticle ink shows relatively high electrical resistivity, approximately two to ten times greater than those of the bulk metal materials [11]. The high resistivity of printed metallic nanoparticles patterns is due to the defects and gaps in the printed tracks, e.g., different coefficients of thermal expansion between the printed patterns and substrates, and the low electrical contacts are formed between the particles. These problems undermine the conductivity of the printed electronics. On the other hand, as the AJP technology is based on the accumulation of nanoparticles, the granular boundaries and defects in the structure will affect the flexibility of the printed tracks [12], ultimately reducing the electrical performance of the fabricated electronic components dramatically.

To ensure good electrical conductivity of metallic printed structures, a variety of metallic-nanoparticle based colloids have been used as inks. Highly conductive metals with stable oxidation states, such as silver (Ag) and gold (Au), are best for utilization in conductive inks. Currently, Ag is the most widely used material in printed electronics (i.e., flexible sensors) [13], however, due to their intrinsic rigidity, brittle failures occur because of the highly concentrated stress areas [14,15]. Consequently, the mechanical

1   SCHOOL OF MECHANICAL AND ELECTRONIC ENGINEERING, SUZHOU UNIVERSITY, SUZHOU 234000, CHINA
2   SCHOOL OF MECHANICAL AND AEROSPACE, NANYANG TECHNOLOGICAL UNIVERSITY, SINGAPORE 639798, SINGAPORE
3   DEPARTMENT OF 3D PRINTING, KOREA INSTITUTE OF MACHINERY & MATERIALS, DAEJEON 34103, REPUBLIC OF KOREA

*   Corresponding author: jpchoi@kimm.re.kr

flexibility and electrical performance of printed Ag flexible sensors require improvements. To address these problems, a more advanced AJP material needs to be developed by using metal composites reinforced with carbon nanomaterials. In particular, carbon nanotubes (CNTs) have inherent advantages including high current-carrying capability, thermal conductivity, chemical stability, and mechanical strength, which are considered to have great potential to improve the flexibility and conductivity of the printed tracks [4, 16-19]. Herein, in order to further enhance the conductivity and flexibility, CNTs added to the Ag ink to prepare Ag/CNTs composites for the fabrication of customized temperature sensors by the AJP process.

2. Experimental

In this study, an Optomec® AJ200 aerosol jet printer with an ultrasonic atomizer was used to produce printed samples. As shown in Fig. 1(a), the AJP process consists of three main stages [20]. Initially, the functional ink maintained at 25°C is atomized into an aerosol stream by an ultrasonic atomizer. Then, a carrier gas stream will entrain the ink aerosol to the print head. After further enwrapped and accelerated by a sheath gas flow, the focused ink aerosol would impact the moving platform (4 mm below), and a single line is printed onto the substrate. In the present research, an Ag nanoparticle ink diluted 2:2:1 by volume with de-ionized water and CNTs was used in the experiments.

To assess the printed line quality, edge roughness and line overspray are evaluated. As shown in Fig. 1(b), the mean line is the reference line used to calculate the edge roughness, defined as

$$\overline{w} = \frac{1}{L}\int_0^L w(x)\,dx \qquad (1)$$

where $w(x)$ is the line width at the xth column of the discretized line edges and L is the length of the printed line. Additionally, the mean edge roughness is defined as

$$R_m = \sqrt{\frac{1}{2L}\int_0^L \left(\delta_{upper}^2(x)+\delta_{lower}^2(x)\right)dx} \qquad (2)$$

where δ_{upper} and δ_{lower} are the deviation between the mean line edge and the corresponding actual edge, respectively. Based on

the determined mean lines, the line overspray O_{sp} is defined to evaluate the mean distance between the overspray spots and the upper- and lower-line edges.

$$O_{sp} = \frac{\int_0^L \left(\theta_{upper}(x)+\theta_{lower}(x)\right)dx}{2L} \qquad (3)$$

Here, θ_{upper} and θ_{lower} are the distance between the overspray spots and the corresponding actual line edge, respectively.

The printed line features are influenced by a number of different factors, including the viscosity of the ink, the substrate properties, and the print head configuration. However, as the sheath gas flow rate (SHGFR) and carrier gas flow rate (CGFR) are the key adjustable parameters during the printing process [21,22], they are investigated as the main input parameters of AJP in the optimization process. To explore the design space systematically and identify the optimal process parameters for AJP, Latin hypercube sampling (LHS) is adopted for the initial experimental design in this study [23]. As described in Fig. 1(c), eleven representative experimental points are generated by LHS in a 2D design space; the optimized ranges of SHGFR and CGFR are set to [50,65] sccm and [35,50] sccm, respectively. The sheath gas flow rate and carrier gas flow rate are quoted in standard cubic centimeters per minute (sccm).

3. Results and discussion

To identify the optimal process parameters, the printed line quality was evaluated in the design space. First, a single line (5 mm long) with Ag/CNTs was printed onto a polyimide substrate. In this case, the printing speed, the current of the ultrasonic atomizer, and the nozzle tip diameter were fixed at 1 mm/s, 0.4 mA, and 150 μm, respectively. Fig. 2 illustrates examples of printed line morphologies from different process parameters. The samples of the printed lines from run 3 and run 10 show high roughness and overspray particles, which will significantly reduce the performance of printed electron components. In contrast, the samples of run 5 and run 6 demonstrate a continuous printed line with low roughness and overspray particles, indicating that appropriate process parameters (SHGFR and CGFR) played an important role in the printed line quality [24]. The
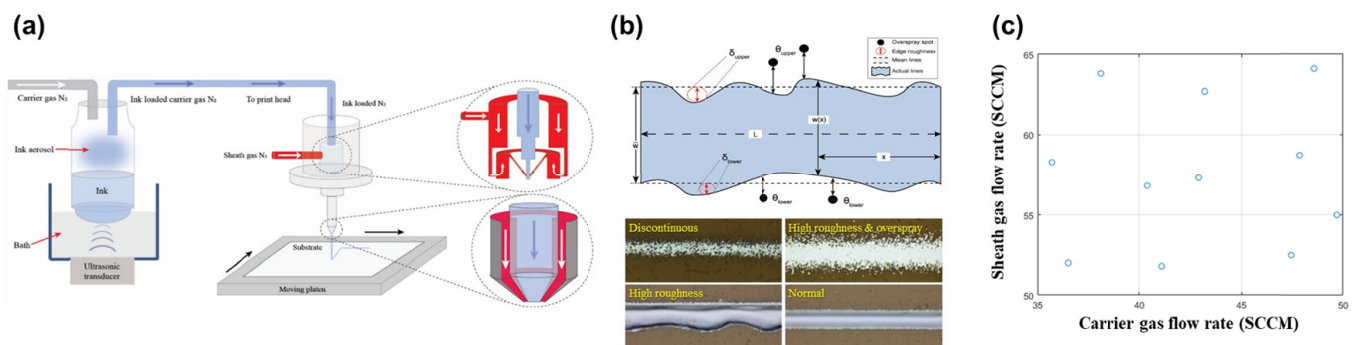

Fig. 1. (a) Working principle of the aerosol jet printing using an ultrasonic atomizer, (b) schematic of the analysis of the printed line quality, (c) selected process parameters in the design space
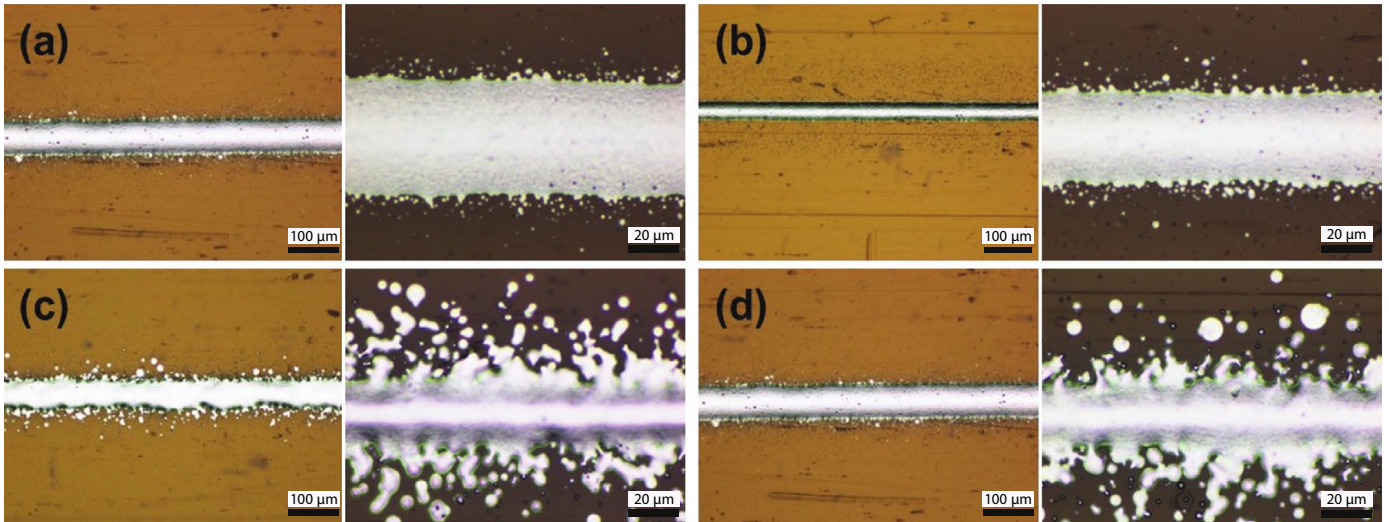
Fig. 2. Printed line morphologies of samples of (a) run 5, (b) run 6, (c) run 3, and (d) run 10

comparison of the experimental results demonstrates that run 6 can print better line samples than the other representative design points. Therefore, in this research, the sample of run 6 (Sheath gas flow rate: 57.3 sccm, Carrier gas flow rate: 42.9 sccm) provided the optimal process parameters in the design space for the fabrication of a temperature sensor.

Based on the above results, the process parameters used for the sample of run 6 were selected to fabricate the customized temperature sensor using AJP technology. Initially, the temperature sensor was designed based on AutoCAD (Autodesk) software (Fig. 3(a)). Then, the sensor was printed onto the substrate. After which, the deposited temperature sensors were post-processed (i.e., sintered) in an oven at 200°C to enhance the electrical conductivity further, as depicted in Fig. 3(b). For comparison, pure Ag ink was also prepared to produce identical temperature sensors under optimal processing conditions from a previous study [25].

Fig. 3(c) and (d) show the morphologies of the lines printed with pure Ag ink and with the Ag/CNTs after sintering, respectively. The sizes of the Ag nano-particles in Fig. 3(c) were in the approximately range of 20-40 nm, and many defects and granular boundaries can be found on the surface of the printed lines. Due to the defects and boundaries of the printed pure Ag line, the sintered Ag particles would separate into discontinu-

ous blocks, which will reduce the continuity and increase the interfacial resistance of the printed line dramatically. In contrast, as presented in Fig. 3(d), CNTs can be found in the printed line based on the proposed mixture design. As CNTs bundles serve as bridges to connect the defects and granular boundaries in the printed line, new and shortened paths are created, through which electrons can pass, thus enhancing the conductivity of the printed lines. Moreover, as the CNT bridges can connect the granular boundaries between the blocks, the flexibility can be improved compared to the lines printed without CNTs.

In order to investigate the mechanical flexibility of the printed sensors, a bending test was conducted; the temperature sensors printed with pure Ag and Ag/CNTs were subjected to repeated 3000-5000 bending cycles at bending radii (r) of 5 (1.02% strain) and the resistance variations were calculated. Fig. 4(a) illustrates the bending test results of line samples printed with the Ag/CNTs ink under the optimized working parameters. The CNTs can serve as bridges to connect the defects/granular boundaries in the printed Ag tracks after sintering, which will enhance the conductivity of the printed electronics [26]. Furthermore, the connections between the CNTs and Ag nanoparticles resulted in a rapid electron flow channel by lowering the Schottky barrier at the interface between the CNTs and the metal atoms [27,28]. Therefore, compared to the bending test results of the
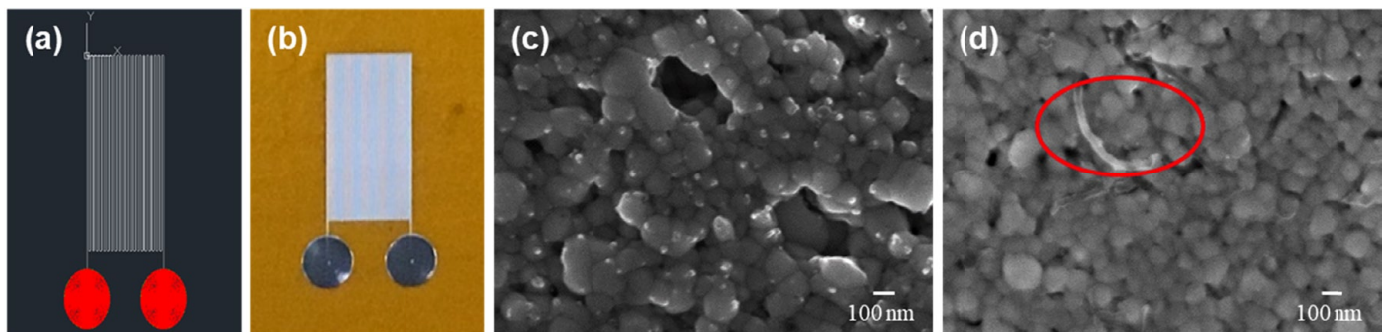

Fig. 3. Temperature sensor: (a) CAD design and (b) fabricated part. SEM image of a printed temperature sensor after sintering at 200°C: (c) pure Ag and (b) Ag/CNTs
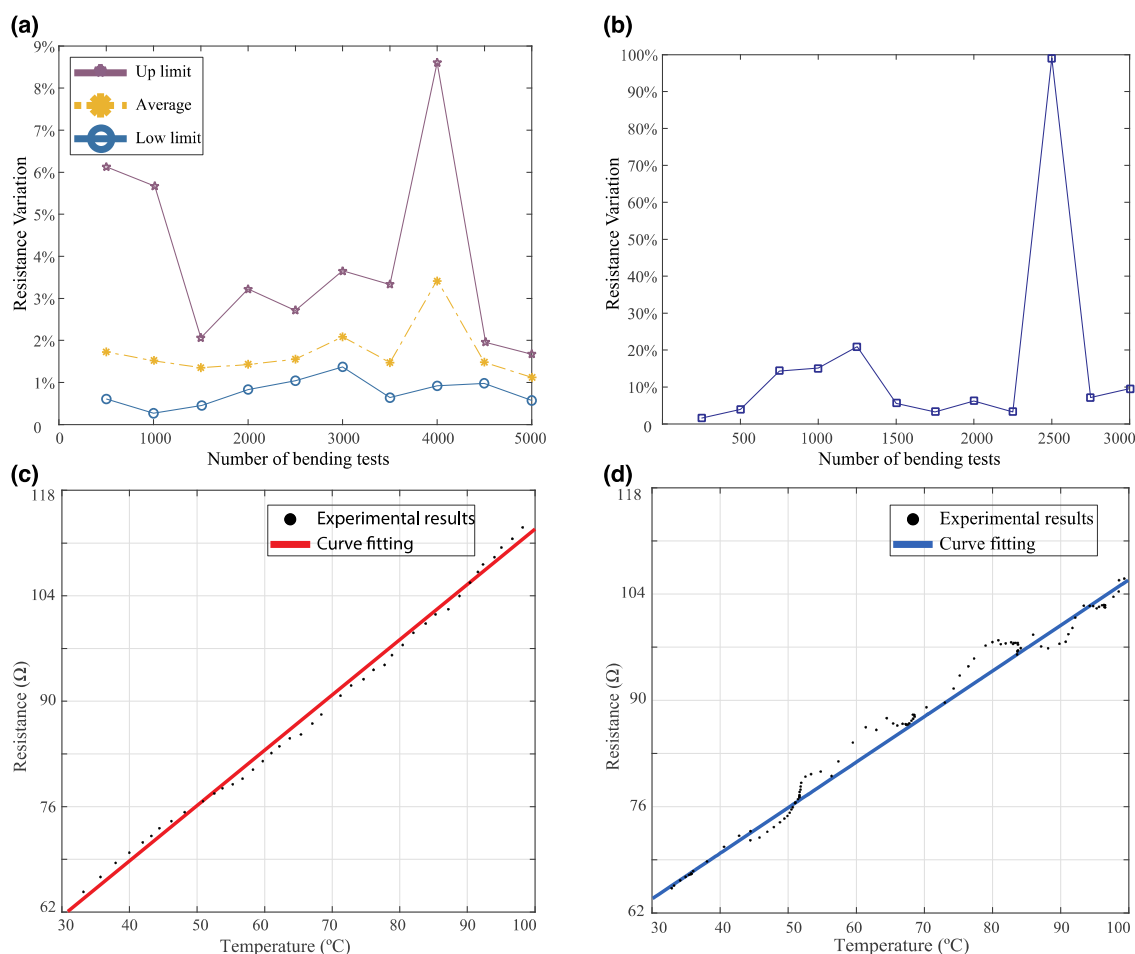
(a)

(b)

(c)

(d)

Fig. 4. Comparison of bending test and calibration results of printed samples based on (a,c) the Ag/CNTs ink and (b,d) the pure Ag nanoparticle ink

pure Ag nanoparticle lines (Fig. 4(b)), the resistance variation under repeated bending tests demonstrated the superior stability and mechanical flexibility of the CNTs mixtures.

After the fabrication process, the temperature sensors that were produced using the Ag/CNTs ink and pure Ag nanoparticle ink were both calibrated in the temperature measurement range from 25°C to 100°C. As depicted in Fig. 4(c), the resistance of the printed Ag/CNTs temperature sensor increases in a reasonably linear manner with the temperature. Instead, due to the greater fluctuation, the resistance of the temperature sensor printed with pure Ag demonstrates a weak linear relationship with the temperature changes (Fig. 4(d)). In addition to the excellent linearity, the printed Ag/CNTs temperature sensor reveals higher temperature sensitivity than the pure Ag temperature sensor, which guarantees the accuracy of temperature measurement. This phenomenon, a favorable increase in electrical conductivity, could be ascribed to the enhancement of effective electron transport due to CNTs as reinforcement materials in the matrix [29,30].

fabricated based on the optimized process parameters of the AJP technology. The flexibility and electrical performance of the printed temperature sensors using Ag/CNTs nanocomposite ink demonstrate good sensitivity in extended measurements. This can mainly be attributed to the addition of CNTs, which served as conductive filler and reinforcement in the Ag/CNTs mixture. Consequently, the novel Ag/CNTs nanocomposite ink can potentially be used in high-performance electronic devices such as flexible electronics created by the AJP process.

4. Conclusions

In an effort to improve the flexibility of the printed tracks, an Ag/CNTs nanocomposite ink is developed in this study. Furthermore, customized temperature sensors are designed and

REFERENCES

[1] J. Chang, X. Zhang, T. Ge, J. Zhou, Org. Electron. **15**, 701 (2014).

[2] G. Cadilha Marques, S.K. Garlapati, S. Dehm, S. Dasgupta, H. Hahn, M. Tahoori, Appl. Phys. Lett. **111**, 102103 (2017).

[3] H.S. Kim, J.S. Kang, J.S. Park, H.T. Hahn, H.C. Jung, J.W Joung, Compos. Sci. Technol. **69**, 1256 (2009).

[4] S. Park, M. Vosguerichian, Z. Bao, Nanoscale **5**, 1727 (2013).

[5] J. Zikulnig, C. Hirschl, L. Rauter, M. Krivec, H. Lammer, F. Riemelmoser, A. Roshanghias, Flex. Print. Electron. **4**, 015008 (2019).

[6] S.N. Kwon, S.W. Kim, I.G. Kim, Y.K. Hong, S.I. Na, Adv. Mater. Technol. **4**, 1800500 (2019).

[7] R. Liu, H. Ding, J. Lin, F. Shen, Z. Cui, T. Zhang, Nanotechnology **23**, 505301 (2012).

[8] M. Ha, J.W.T. Seo, P.L. Prabhumirashi, W. Zhang, M.L. Geier, M.J. Renn, C.H. Kim, M.C. Hersam, C.D. Frisbie, Nano Lett. **13**, 954 (2013).

[9] A.A. Gupta, A. Bolduc, S.G. Cloutier, R. Izquierdo, 2016 IEEE International Symposium on Circuits and Systems (ISCAS), 866 (2016).

[10] S. Vella, C.S. Smithson, K. Halfyard, E. Shen, M. Chrétien, Flex. Print. Electron. **4**, 045005 (2019).

[11] S.K. Eshkalak, A. Chinnappan, W. Jayathilaka, W.A.D.M. Jayathilaka, M. Khatibzadeh, E. Kowsari, S. Ramakrishna, Appl. Mater. Today. **9**, 372 (2017).

[12] D. Zhao, T. Liu, J.G. Park, M. Zhang, J.M. Chen, B. Wang, Microelectron. Eng. **96**, 71 (2012).

[13] A. Kamyshny, S. Magdassi, Chem. Soc. Rev. **48**, 1712 (2019).

[14] W.J. Hyun, S. Lim, B.Y. Ahn, J.A. Lewis, C.D. Frisbie, L.F. Francis, ACS Appl. Mater. Interfaces **7**, 12619 (2015).

[15] K.S. Siow, J. Alloys Compd. **514**, 6 (2012).

[16] B.Q. Wei, R. Vajtai, P.M. Ajayan, Appl. Phys. Lett. **79**, 1172 (2001).

[17] E. Brown, L. Hao, J.C. Gallop, J.C. Macfarlane, Appl. Phys. Lett. **87**, 023107 (2005).

[18] G.L. Goh, S. Agarwala, W.Y. Yeong, Adv. Mater. Interfaces **6**, 1801318 (2019).

[19] S. Yao, Y. Zhu, Adv Mater. **27**, 1480 (2015).

[20] H. Zhang, S.K. Moon, ACS Appl. Mater. Interfaces **13**, 53323 (2021).

[21] M. Smith, Y.S. Choi, C. Boughey, S. Kar-Narayan, Flex. Print. Electron. **2**, 015004 (2017).

[22] H. Zhang, S.K. Moon, Int. J. of Precis. Eng. and Manuf-Green. Tech. **7**, 511 (2020).

[23] H. Zhang, J.P. Choi, S.K. Moon, T.H. Ngo, J. Mater. Process. Technol. **285**, 116779 (2020).

[24] R.R. Salary, J.P. Lombardi, M. Samie Tootooni, R. Donovan, P.K. Rao, P. Borgesen, M.D. Poliks, J. Manuf. Sci. Eng. **139**, 021015 (2017).

[25] H. Zhang, J.P. Choi, S.K. Moon, T.H. Ngo, Addit. Manuf. **33**, 101096 (2020).

[26] Y. Oh, D. Suh, Y. Kim, E. Lee, J.S. Mok, J. Choi, S. Baik, Nanotechnology **19**, 495602 (2008).

[27] V. Vitale, A. Curioni, W. Andreoni, J. Am. Chem. Soc. **130**, 5848 (2008).

[28] D.R. Kauffman, A. Star, Nano Lett. **7**, 1863 (2007).

[29] V. Gopee, O. Thomas, C. Hunt, V. Stolojan, J. Allam, S.R.P. Silva, ACS Appl. Mater. Interfaces **8**, 5563 (2016).

[30] D. Zhao, T. Liu, M. Zhang, R. Liang, B. Wang, J. Allam, S.R.P. Silva, Smart Mater. Struct. **21**, 115008 (2012).